Journal of Advances and Scholarly Researches in Allied Education
Vol. 19, Issue No. 4, July-2022, ISSN 2230-7540

Characteristics of NIO Compound Material used in PV Cells, EC Devices, UV Photodetectors, and Gas Sensors

Reetu[1]*, Dr. Pradeep Kumar[2]

[1] Research Scholar, Sunrise University

[2] Assistant Professor, Sunrise University

Abstract - Nickel oxide (NiO) thin films were developed on soda lime glass using radio-frequency magnetron sputtering at growth (substrate) temperatures ranging from room temperature (RT) to 400 °C. Modifications in structure, morphological, electrical, and optical properties were tracked as the substrate temperature varied. The XRD pattern shows that at 100 °C, the (2 0 0) preferred orientations predominate in the film. Nonetheless, EDX showed that NiO was decomposing all during the development of samples at high temperatures, causing the (2 0 0) peak intensity to gradually decrease. The grains were evenly spread, with a maximum grain size of 19.43 nm, as determined by FESEM examination of the surface morphology. In accordance with the XRD results, we find that raising the growth temperature significantly reduces crystal quality and increases grain size. Maximum scanning probe microscopy (SPM) observed surface roughness (1.232 nm) occurs at room temperature. It was discovered that increasing the substrate temperature greatly decreased the electrical resistivity, from 2150 Ω cm to 72 Ωcm. Transmission tests of light through NiO sheets show that the optical bandgap narrows from 3.8 to 3.2 eV when the substrate is heated. The results raise the possibility that NiO films might be employed in solar energy systems.

Keywords - Growth, Temperature, Photovoltaic Properties, Nio, Thin Films

----------X----------

INTRODUCYTION

Thin films may be deposited using sputtering, a physical vapor deposition (PVD) technique. In this process, material is ejected from a "target" onto a "substrate" like a silicon wafer. During the deposition process, ion or atom bombardment may cause the deposited material to be re-emitted, a process known as reuttering. The energy distribution of spat atoms is generally many tens of eV (100,000 K) broad. Since only a tiny percentage of the ejected particles are ionized (usually on the order of 1 percent), the sputtered ions might fly in straight lines away from the target and crash into the substrates or vacuum chamber with enough force to cause reuttering. Or, at greater gas pressures, the ions randomly travel toward the substrates or vacuum chamber wall, hit with the gas atoms that function as a moderator, and then condense. By adjusting the pressure of the surrounding air, you can create effects ranging from a high-energy ballistic hit to a low-energy thermalized motion.

The gas used for sputtering is typically an inert gas like argon. The atomic weight of the sputtering gas should be near to that of the target for effective momentum transfer; hence, neon is preferred for sputtering light elements, while krypton or xenon are used for sputtering heavy elements. It is also possible to sputter substances using reactive gases. Depending on the conditions, the chemical may either develop on the substrate, in mid-air, or on the target surface. Although sputter deposition is a complicated process, specialists have a great deal of control over the film's development and microstructure because to the wide range of available parameters.

To fabricate a thin-film solar cell, a photovoltaic material is deposited as a thin layer (thin film, or TF) onto a substrate Conventional crystalline silicon (c-Si) based solar cells employ wafers that may be up to 200 m thick, whereas thin-film solar cells are often just a few nanometers (nm) to a few microns (m) thick. CdTe, CIGS, and amorphous thin-film silicon (a-Si, TF-Si) are only a few of the commercial technologies that employ thin-film solar cells.

Single- or multi-crystalline silicon solar cells, which have been around the longest, are considered to be

the first generation of solar cells because of the active (sunlight-absorbing) layers utilized in their production. This is the standard method utilized in most PV systems today. The vast majority of current solar cells are second-generation thin-film varieties, constructed from atomically thin layers of materials like amorphous silicon (a-Si), cadmium telluride (CdTe), copper indium gallium selenide (CIGS), or gallium arsenide (GaAs). Third-generation solar cells, often known as emerging solar cells, are constructed from novel, less conventional materials. Perovskite solar cells, dye-sensitized solar cells, quantum dots, organic solar cells, and CZTS thin-film solar cells are all examples of such cutting-edge thin-film technology.

LITERATURE REVIEW

Adjogri, Shadrack et.al (2021). As late as 2015, chalcogenide perovskites, a novel semiconductor, were still thought to have promise as a practical solar cell material. Finding safer alternatives to the top performing hybrid lead iodide perovskite (MAPbI3) was critical. Consequently, chalcogenide perovskites and perovskite-based chalcothallite thin-film light absorbers have recently been considered as options for solar applications. In order to create novel hybrid perovskites, dimensionality tailoring and compositional substitution approaches have been widely used. The optoelectronic properties of chalcogenide perovskites and perovskite-based chalcothallite are discussed in detail in relation to their potential use in future solar applications.

Kuanr, Sushil et.al (2016). Using electron beam physical vapor deposition (EB-PVD), depositing a thin layer of composite materials remains challenging. This paper describes the EB-PVD deposition of NiO-CeO2 composites (30/70 wt.%) on a quartz substrate. Two NiO-CeO2 nanocomposite targets, one compact green and one sintered at 1250°C, were used for the deposition. The relevance of the physical nature of the deposition process was shown by the fact that the mean crystallite size of the produced thin films was in the range of 20 to 25 nm, even though the targets varied in crystallite size from 11 to 45 nm and relative density from 44 to 96 percent. Although the sintered targets had a crystalline structure and a similar concentration of elements, the thin films produced from them demonstrated a change from an amorphous to a crystalline structure. After deposition, the as-deposited film was annealed at 800 degrees Celsius to produce a CeO2- and NiO-based polycrystalline structure. By monitoring the preferred orientation toward (111) and (200) planes, respectively, when pure CeO2 or NiO was utilized as a target for deposition, it was shown that adatoms influence the evaporation and growing process of NiO-CeO2 composite. Composite oxide thin film development is shown to be energy-dependent on the intensity of the electron beam gun.

Zakutayev, Andriy. (2017). Photovoltaic solar cells are on track to provide more than 1% of global energy consumption because to recent breakthroughs in commercialization. However, additional research into solar techniques without scaling restrictions is necessary if they are to provide more than 10% of the world's electricity. This review paper from 2017 summarizes key findings from the last several years of research into innovative solar absorber materials. While CdTe, Cu(In,Ga)Se2, and CH3NH3PbI3 have been around for a while, newer absorbers like SnS, Sb2Se3, Cu2SnS3, and CuSb2Se2 are gaining a lot of traction in the solar cell business. The present situation of academic publication and performance is then analyzed, and some promising avenues for future research are highlighted.

Ashokan, Ajith et.al (2018). Bulk-heterojunction organic solar cells' performance is highly dependent on the geometry of the active layer. The solution temperature-dependent aggregation properties of a variety of polymer donors have recently been used to provide an effective mechanism for morphology control in high-efficiency devices. The influence of solution temperature-dependent aggregation on the packing and electrical properties of polymers in the solid state is investigated here using an approach that combines molecular dynamics simulations with long-range corrected density functional theory calculations. We consider two representative polymer systems: (i) PffBT4T-2OD (poly[(5,6-difluoro-2,1,3-benzothiadiazol-4,7-diyl)-alt-(3,3'''-di(2-octyldodecyl)-2,2';5',2'';5'',2'''-quaterthiophen-5,5'''-diyl)]), and (ii) PBT4T-2OD (poly[(2,1,3-benzothiadiazole-4,7-diyl)-alt-(3,3'''-di(2-octyldodecyl)-2.2';5',2'';5'',2'''-quarterthiophen-5,5'''-diyl)]), where the fluorine atoms on the benzothiadiazole moieties of PffBT4T-2OD are replaced with hydrogen atoms.

Pakštas, Vidas et.al (2020). This study takes a methodical look at how the thickness of the CdS layer affects the composition and structure of CZTSSe films, as well as the photovoltaic efficiency of superstrate solar cell devices. Because of the selenization of the CZTS films, Cd diffuses into the absorbent layer. This alteration in lattice properties and crystallinity causes an inhomogeneous distribution of S and Se ions over the thickness of the CZTSSe layer and leads to the production of the CZCTSSe kesterite phase. On the other hand, it is suggested that a rise in Cd content for a given quantity is responsible for the enhanced crystallinity, shape, and maybe graded band-gap of CZCTSSe films, which in turn improves the device performance characteristics. Superstrate-architecture, spray-pyrolysis-deposited solid-state CZTSSe solar cells achieve a remarkable 3.3% power conversion efficiency.

EXPERIMENTAL PROCEDURE

At room temperature, thin films of NiO were deposited by RF magnetron sputtering over clean soda lime glass A series of soapy water, distilled water, methanol, isopropanol, and distilled water was used to ultrasonically clean the substrates. The

substrates were then cleaned with acetone and dried in a stream of nitrogen gas. Finally, organic residues were eliminated by exposing substrates to UV light for 30 minutes. The raw material for this sputtering target was a stoichiometric NiO target NiO sputtering target dimensions were 50 mm in diameter and 5 mm in thickness. The target and substrate separation were maintained at 14 centimeters. The target was pre-sputtered for 15 minutes at 50 W electricity to remove any contaminants from the surface. The conditions for the deposition were held constant at 5 106 Torr for the base pressure, 28 m Torr for the working pressure, 50 W for the sputtering power, and 90 minutes for the deposition duration. The mass flow controller set the reactive gas flow rate to 4 sccm, and the gas was high-purity Ar (99.9999%). Throughout the sputtering process, the substrate holder rotated at a steady 10 rpm. The substrates were heated for 45 minutes at the desired deposition temperature of 100-400 °C before being subjected to sputtering.

DATA ANAYSIS

Structural analysis of the NiO films

Figure 1(a) displays the XRD pattern of NiO thin films at various substrate temperatures with diffraction angles ranging from 20° to 70°. Diffraction patterns of RF-sputtered NiO films demonstrate that, with the exception of the sample sputtered at 400 °C, all samples display two diffraction peaks at 43.3° and 62.5°, respectively, corresponding to NiO (2 0 0) and Ni (2 2 0) orientations. It can be shown by comparing the XRD pattern from this research to the reference XRD spectrum found in JCPDS card No. 00-047-1049 that the generated polycrystalline NiO layer crystallizes in a cubic structure. The preponderant maximum amplitude

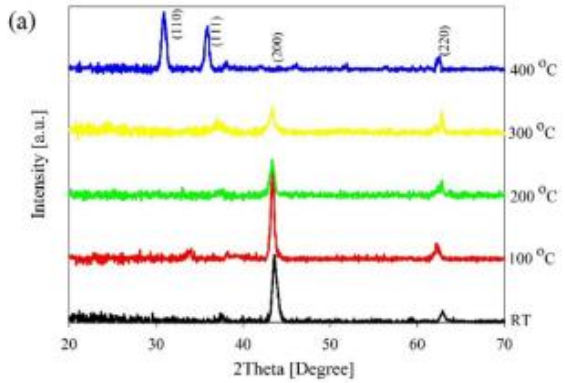

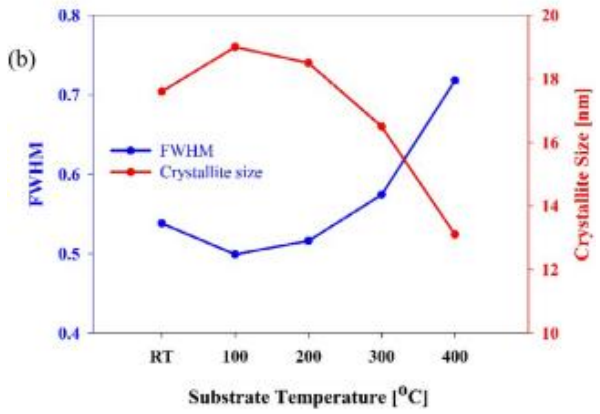

Fig. 1. Structural properties of the NiO thin films at different substrate temperatures, (a) XRD pattern, (b) variations of FWHM, and crystallite size.

occurs at a substrate temperature of 100 °C, demonstrating excellent crystallinity and a high degree of orientation. Substrate temperature has a linear relationship with the intensity of the (2,0,0) diffraction peak in NiO. NiO films completely lose their crystal clarity at 400 °C, with diffraction peaks appearing at 35.89° and 30.92° along the (1 11 1) and (1 1 0) planes. High thermal energy accessible to the adatoms of NiO films at substrate temperatures over 100 °C degrades the crystallinity of NiO films. This outcome may be explained by the establishment of a preferential orientation along the (2 0 0) plane due to limited atomic mobility at low substrate temperature. NiO atoms receive extra energy and preferentially reorient themselves along the (1 1 1) and (1 1 0) planes when the substrate temperature rises. The NiO target was sputtered using radio frequency in this experiment. Thus, at high substrate temperature, NiO is partly separated into Ni and O metals. The crystal quality of NiO thin films degrades as a result of this process. These findings correlate well with previous research showing that high substrate temperatures reduce the crystallinity of several thin films. The XRD data was used to determine a number of structural factors, such as crystallite size, FWHM, strain, dislocation density, microstrain, and lattice parameter. Changes in crystallite size and full width at half maximum (FWHM) of NiO diffraction peaks along the (2 0 0) plane as a function of substrate temperature are shown in Fig. 1(b). Debye-Scherrer's equation was used to get the typical crystallite size (dhkl).

$$d_{hkl} = k\lambda/(\beta cos(2\theta))$$

λ the Bragg's angle of diffraction, β the full width at half maximum (FWHM) intensity of the primary peak recorded at 2θand a constant k. when seen in Fig. 1(b), when the substrate temperature rises, the NiO crystallite size drops while the full width at half maximum (FWHM) rises. As the substrate temperature was raised from RT to 400 °C, the

crystallite size was found to drop from 19.43 nm to 13.10 nm. This finding is attributed to the disintegration of the NiO thin layer at high substrate temperature, which limits the adatoms' ability to diffuse to the surface. Using Eqs. (2) and (3), we determined the microstrain (ε) and dislocation density (δ) of the NiO thin films.

$$\varepsilon = \beta/(4tan\theta)$$

$$\delta = n/D^2$$

where D is the grain size and n are a near-unity value for the lowest dislocation density possible.

Surface morphology of the NiO films

NiO thin films were examined using FESEM to investigate how their surface shape and cross-sectional view changed throughout a range of substrate temperatures (Fig. 3). The FESEM micrograph clearly reveals the nanoscale grain size of the NiO thin films, the size of which varies dramatically with the substrate temperature. NiO deposited at 100 °C has a homogeneous grain size and good packing density, with an average grain size of 16 nm as shown in a FESEM micrograph. As the substrate temperature rose, the grain size and crystal quality declined precipitously. At 400 degrees Celsius, the grains entirely lose their normal forms. This morphological finding is consistent with the structural investigation of the NiO thin film that has been presented so far. When seen in cross-section, thickness reduces with increasing substrate temperature. As the substrate temperature is raised from RT to 100 °C, the thickness decreases from 100 nm to 60 nm. It's possible that this finding is dependent

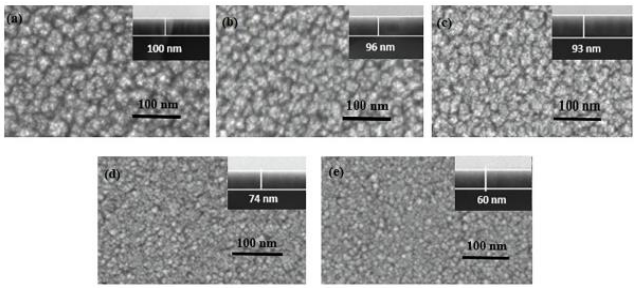

Fig. 3. Top and cross-sectional (inset) views of the NiO thin film at different substrate temperatures: (a) RT, (b) 100 °C, (c) 200 °C, (d) 300 °C, and (e) 400 °C.

Table 1 Hall parameters of the NiO thin films at different substrate temperatures.

Substrate temperature, °C	Carrier concentration, cm^{-3}	Carrier mobility, cm^2/Vs	Resistivity, Ω cm
RT	6.08×10^{14}	6.73	1503
100	2.85×10^{14}	10.20	2150
200	4.49×10^{14}	6.75	2060
300	7.32×10^{15}	2.87	298
400	3.87×10^{16}	2.23	72

Relationship between grain size and film thickness. Figure 4 depicts the substrate temperature's response to the Ni/O ratio. Since NiO atoms disintegrated at high substrate temperature, the ratio of Ni/O grew as temperature rose. This resulted in a decrease in crystal quality. This conclusion is in agreement with the results obtained by Ahmed et al. and Reddy et al. and demonstrates a link between the structural features of NiO thin film. NiO thin films produced on a variety of substrates (Si wafer) were analyzed for surface roughness using SPM. Figure 5 displays 3D SPM pictures of the NiO thin films. Substrate roughness is measured as the root-mean-square (RMS) value as a percentage of typical height. At room temperature (RT), 100 °C, 200 °C, 300 °C, and 400 °C, the substrate's root-mean-square (RMS) surface roughness is measured to be 1.232 nm, 1.046 nm, 0.681 nm, 0.632 nm, and 0.621 nm, respectively. Therefore, the X-ray diffraction (XRD) structural analysis was consistent with the trend of smoother surfaces with increasing substrate temperatures. NiO thin films have better crystalline quality at low temperatures. Inducing more orderly packing of molecules, which may remove holes and dislocations and function as charge traps, is one possible outcome of this characteristic. Fasaki et al. also report comparable results from their experiments.

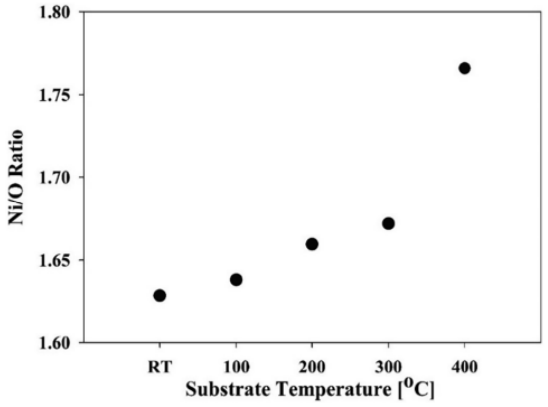

Fig. 4. Variation in the Ni/O ratio as a function of substrate temperature.

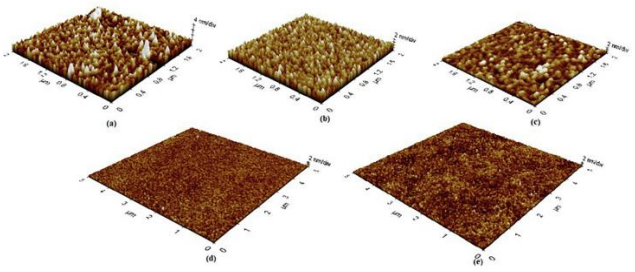

Fig. 5. 3D SPM images of the NiO thin films deposited by RF sputtering at different substrate temperatures: (a) RT, (b) 100 °C, (c) 200 °C, (d) 300 °C, and (e) 400 °C.

Electrical properties of the NiO films

NiO thin films' electrical characteristics are listed in Table 1. NiO's electrical characteristics are strongly influenced by the temperature of the substrate on which it is grown, and this is reflected in the films' p-type conductivity, which ranges from 2.85 x 1014 cm3 to 3.87 x 1016 cm3 when grown at different temperatures. Microstructural flaws in the NiO crystal and the surface chemical reaction account for the temperature dependence of the NiO thin films' electrical conductivity X-ray diffraction analyses show that an increase in substrate temperature leads to a rise in carrier concentration because of a reduction in the crystallinity structure. Eqs. (5) and (6) clarify the connection between carrier concentration, carrier mobility, and resistivity:

Table 2 Urbach energy of the NiO thin films at different substrate temperatures.

Substrate Temperature, °C	Urbach energy, meV
RT	177
100	264
200	250
300	354
400	438

$$\sigma = q\eta\mu_h$$

$$\sigma = \frac{1}{\rho}$$

where σ, ρ, q, η, and μe include things like electrical charge, carrier concentration, and carrier mobility, and their inverses, conductivity and resistivity. According to the formulas, the resistivity is inversely related to the electrical mobility and carrier concentration. NiO thin film carrier mobility rose with increasing substrate temperature and decreased with increasing substrate temperature at first. With further increases in substrate temperature and decreases in resistance, carrier mobility reduced after 100 °C. An increase in dislocation density, as seen in Fig. 2(a), may be to blame for this result since it encourages carrier dispersion and hence lowers carrier mobility. At a substrate temperature of 100 °C, the NiO thin films exhibited a high electrical resistance of 2150 Ω cm. As the substrate temperature was raised to 400 °C, the resistivity of the NiO thin films dropped to 72Ω cm as a result of an increase in carrier mobility. concentration, which is induced by Ni-rich composition through the partial decomposition of NiO at a high substrate temperature.

Table 3 Comparative studies of the experimental results of NiO with previous finding

Target	Sputter-ing gas	Temp, °C	Power, Watt	Substrate	Thickness, nm	Transmittance, %	Band gap, eV	Crystal size, nm	Resistivity, ohm cm
NiO	N_2	RT-400	50	SLG	60-100	60.56-83.69	3.2-3.8	13.10-19.43	72 to 2150
NiO	Ar	RT-300	200	Si	350-358	-	3.72-3.64	20.38-41.29	-
Ni	N_2/O_2	RT-400	250	Fused Si	300	25-70	3.65-3.88		0.028-8.7
NiO	O_2	RT-350	100-200	Corning Glass	-	60%		11.42-18.17	16.7

Optical characteristics of the NiO films

As the substrate temperature rises, there is a little reduction in the NiO thin films' transmittance in the visible spectrum. As the substrate temperature is raised from RT to 400 °C, the transmittance of these films significantly drops from 83.69% to 60.56%. Compositional analysis in this work coincides with an increase in Ni content in NiO thin films, which might explain these results. Due to the high number of grain boundaries and point defects that scatter incoming light, strong scattering is predicted [34]. From the transmission spectra, we were able to derive the optical bandgap (Eg) of the NiO thin films at varying substrate temperatures:

$$(\alpha h\upsilon)^2 = A(h\upsilon - E_g)$$

The evolution of Eg is attributable to changes in the crystallinity and stoichiometry of NiO thin films. In addition, the Burstein-Moss effect might help explain why Eg could vary due to changes in absorption edge and carrier concentration. According to the Brustein-Moss effect, the fermi level of a degraded semiconductor shifts into the conduction band, resulting in an expansion of the energy bands. Since Eg decreases as the substrate temperature rises, the shrinkage effect dominates over the Burstein-Moss effect. The absorption spectrum has an exponential section called the Urbach tail that varies with the absorption coefficient and the photon energy. It indicates the changes in the distance between the valence and conduction band tails. Urbach energy has been linked to film network dysfunction, as described by Rahal et al. For weak photons, the following equation describes the Urbach empirical rule:

$$\alpha = \alpha_o \exp(h\nu/E_u)$$

, where α o is a constant and Eu is the Urbach energy, which varies with temperature, h is the photon energy, and is the absorption coefficient. Slopes of ln(α) against photon energy (hυ) plots have been used to calculate the NiO thin films' Urbach energy. Urbach energy values (Table 2) are calculated from the inverted slope of ln(α) against photon energy (hυ) graphs.

CONCLUSIONS

Soda lime glass was used as the substrate, and thin layers of NiO were formed by RF magnetron sputtering at temperatures ranging from room temperature to 400 °C. The highest peak intensity was achieved at 100 °C, and when the substrate temperature was raised above this point, the crystal quality drastically degraded. As the temperature of the substrate rose, the surface roughness, film thickness, and crystallite size all reduced. Substrate heat likely increased microstrain and dislocation density by relieving stress in the NiO thin film. At high substrate temperature, Ni atomic percentage

rose, suggesting that O may have been broken down. As the substrate temperature rose, the NiO thin film exhibited higher carrier concentration and carrier mobility and lower resistance. At 400 °C, a resistivity of 72 Ω cm was measured. According to the optical characteristics, when the substrate temperature rises, the Urbach energy rises and the optical bandgap decreases. These findings demonstrate that NiO thin film formed at 100 °C has desirable features for use in photovoltaics, especially as the heterojunction material (HTM) of a perovskite solar cell.

REFERENCES

1. Adjogri, shadrack & meyer, edson. (2021). Chalcogenide perovskites and perovskite-based chalcohalide as photoabsorbers: a study of their properties, and potential photovoltaic applications. Materials. 14. 7857. 10.3390/ma14247857.
2. Kuanr, sushil & krishna moorthy, suresh babu. (2016). Structural and growth aspects of electron beam physical vapor deposited nio-ceo2 nanocomposite films. Journal of vacuum science & technology a: vacuum, surfaces, and films. 34. 021507. 10.1116/1.4937357.
3. Zakutayev, andriy. (2017). Brief review of emerging photovoltaic absorber materials. Current opinion in green and sustainable chemistry. 4. 10.1016/j.cogsc.2017.01.002.
4. Ashokan, Ajith & wang, tonghui & ravva, mahesh kumar & bredas, jean-luc. (2018). Impact of solution temperature-dependent aggregation on the solid-state packing and electronic properties of polymers for organic photovoltaics. Journal of materials chemistry c. 6. 10.1039/c8tc05378b.
5. Pakštas, vidas & grinciene, giedre & kamarauskas, egidijus & giraitis, raimondas & skapas, martynas & selskis, algirdas & juškėnas, remigijus & niaura, gediminas & franckevičius, marius. (2020). Impact of cds layer thickness on the composition, structure and photovoltaic performance of superstrate cztsse solar cells. Solar energy. 207. 1231-1239. 10.1016/j.solener.2020.07.052.
6. Huang, jinsong & yuan, yongbo & shao, yuchuan & yan, yanfa. (2017). Understanding the physical properties of hybrid perovskites for photovoltaic applications. Nature reviews materials. 2. 17042. 10.1038/natrevmats.2017.42.
7. Rezvani, maryam & gholami, aslan & gavagsaz-ghoachani, roghayeh & zandi, majid. (2023). A review on the effect of dust properties on photovoltaic solar panels' performance. Journal of renewable and new energy. 10. 198-211. 10.52547/jrenew.10.1.198.
8. Vidyanandan, k.v. (2017). An overview of factors affecting the performance of solar pv systems. Energy scan (a house journal of corporate planning, ntpc ltd.). 27. 2-8.
9. Roa, simon & sandoval, myrna & cortes, maria & manidurai, paulraj & suárez, sergio. (2021). Potential photovoltaic properties of thin film solar cells based on chemically deposited zno/pbse junctions. Journal of alloys and compounds. 871. 159559. 10.1016/j.jallcom.2021.159559.
10. Liu, xueqing & yue, song & lu, luyi & li, jianlan. (2022). Mechanism underlying the effect of physical properties on the dynamic behaviours and erosion characteristics of particles on solar photovoltaic panels. Chemical papers. 76. 10.1007/s11696-022-02175-3.
11. Pfannmöller, martin & kowalsky, wolfgang & schröder, rasmus. (2013). Visualizing physical, electronic, and optical properties of organic photovoltaic cells. Energy & environmental science. 6. 2871. 10.1039/c3ee41773e.
12. Hossain, m. Khalid & Toki, gaze farhan & samajdar, dip & rubel, mirza & Mushtaq, Muhammad & Islam, md. Residual & Rahman, md & Bhattarai, sagar & bencher if, Hicham & k. A. Mohammed, Mustafa & Pandey, Rahul & Madan, Jaya. (2023). Photovoltaic performance investigation of cs3bi2i9-based perovskite solar cells with various charge transport channels using dft and scaps-1d frameworks. 37. 7380–7400. 10.1021/acs.energyfuels.3c00540.
13. Guerra, noemi & guevara, marco & palacios arias, césar & crupi, felice. (2018). Operation and physics of photovoltaic solar cells: an overview. I+d tecnológico. 14. 84-95. 10.33412/idt. V14.2.2077.
14. Almukhtar, hussam & lie, tek tjing & al-shohani, wisam & anderson, timothy & al-tameemi, zaid. (2023). Comprehensive review of dust properties and their influence on photovoltaic systems: electrical, optical, thermal models and experimentation techniques. Energies. 16. 3401. 10.3390/en16083401.
15. Sharma, shruti & jain, kamlesh & sharma, ashutosh. (2015). Solar cells: in research and applications—a review. Materials sciences and applications. 06. 1145-1155. 10.4236/msa.2015.612113.

Corresponding Author

Reetu*

Research Scholar, Sunrise University